CHAPTER 7

Effect of Initial Excess Pore Pressures on Unsaturated Consolidation

7.1 INTRODUCTION

The previous chapters deal with the various aspects of consolidation for the completely saturated soil. However, in most construction sites, especially in arid and semi-arid zones, the consolidating layer remains in a partially saturated condition. Predicting consolidation for unsaturated soil is more complex due to its three-phase system (soil solid, air, and water). There are several consolidation theories (Biot 1941; Blight 1961; Scott 1963; Barden 1965; Barden 1974; Liakopoulos 1965; Fredlund and Morgenstern 1976; Fredlund and Hasan 1979) for predicting the transient fluid flow and the subsequent deformation on the unsaturated soils. Fredlund and Hasan's (1979) 1-D unsaturated consolidation equation is widely accepted and comprehensively used for predicting the tempo-spatial variation of excess pore pressure dissipations in the vadose zone. The nonlinear partial differential equations of Fredlund and Hasan (1979) were further converted into linear form (Fredlund and Rahardjo 1993) and extended to solve two-dimensional (Dakshanamurthy and Fredlund 1980) and three-dimensional (Dakshanamurthy et al. 1984) problems. Considering Fredlund and Rahardjo's (1993) diffusion equations, the consolidation phenomena in the vadose zone were further analyzed (Qin et al. 2008; Qin et al. 2010; Shan et al. 2012; Shan et al. 2013; Ho et al. 2014; Ho and Fatahi 2016; Zhou et al. 2014) by considering time-dependent loading and mixed drainage boundaries. Qin et al. (2008, 2010) used Laplace transformation for the consolidating layer subjected to instantaneous and exponential loadings. Shan et al. (2012, 2013) proposed

exact solutions for various loading types under different drainage conditions. Ho et al. (2014) and Ho and Fatahi (2016) offered solutions for single and double drainage boundary conditions using the Eigen-function expansion method. Zhou et al. (2014) linearize the nonlinear PDEs and obtain analytical solutions.

Almost all these studies considered the load-induced excess pore pressures to be distributed uniformly. As explained in Chapter 3, the initial pore pressures developed at the moment of load application often exhibit various shapes- symmetric or asymmetric, linear or non-linear - but they are typically not uniform. Zhou et al. (2013) presented analytical solutions for uniform, trapezium, and half-sine (increasing) pore water pressure distributions in unsaturated soil under various loading conditions. Zhou and Zhao (2014) proposed solutions for trapezium, and skewed pore water pressure distributions under constant and time-dependent loading with single and double drainage boundary conditions. The existing literature indicates that only a few studies have explored non-uniform pore pressure in consolidation, and these studies have considered a very limited range of initial pore pressure shapes. It is also to be noted that in contrast to the saturated soils, the application of load induces pore water and pore air pressures. The author did not encounter any studies on unsaturated consolidation that consider a nonuniform initial pore air pressure. This may be attributed to the fact that the dissipation of pore air pressure is more rapid than the pore water pressure. This chapter addresses these gaps by conducting a detailed 1-D consolidation analysis of homogeneous unsaturated clayey soil, considering various shapes of pore pressure distributions, and altering the geometric variables of each distribution.

7.2 PROBLEM STATEMENT

A constant uniform load of magnitude q is applied over a horizontal surface of an unsaturated clayey stratum of height H, as shown in Fig.7.1. The water table remains at or

below the bottom of the clayey layer. Unlike saturated soil, the overall deformation of the unsaturated clay layer depends on two stress state variables, namely, net normal stress ($\sigma - u_a$) and matric suction (u_a–u_w); where, u_a and u_w are the excess pore air pressure (PAP) and pore water pressure (PWP) at any arbitrary stage. Upon the application of the instantaneous load, *initial excess pore-air* (u_{a0}) and *pore-water* (u_{w0}) *pressures* are generated in an undrained condition. The magnitude of u_{w0} and u_{a0} depends on the compressibility parameters ($m_{1k}^s, m_2^s, m_{1k}^w, m_2^w$). Appendix E1 presents the definitions of the compressibility parameters. The impact of net normal stress is more on the void ratio, whereas, the matric suction is more effective in changing the water content; symbolically, $m_{1k}^s > m_2^s$ and $m_2^w > m_{1k}^w$.

Obeying Fredlund and Hasan (1979), the expressions of u_{a0} and u_{w0} are obtained with the suitable application of the compressibility equations of the air-water mixture, and the constitutive relations corresponding to the soil-structure phase and the air phase., and Appendix E2 summarizes the derivation of u_{w0} and u_{a0}. For this chapter, the derived u_{w0} and u_{a0} are treated as the maximum values and are symbolized with, $u_{w0,max}$ and $u_{a0,max}$.

To impose the non-uniform pore pressure distributions in the numerical computation, the $u_{w0,max}$ and $u_{a0,max}$ are distributed (identically) in the space in the same manner as the applied load (q) was distributed for the saturated case. The distributions of $u_{w0}/u_{w0,max}$ (or, $u_{a0}/u_{a0,max}$) are treated the same as u_0/q, as given in Chapter 3. Along with the conventional rectangular distribution (Case A), nine other non-uniform distributions (Case B to Case J) are assessed.

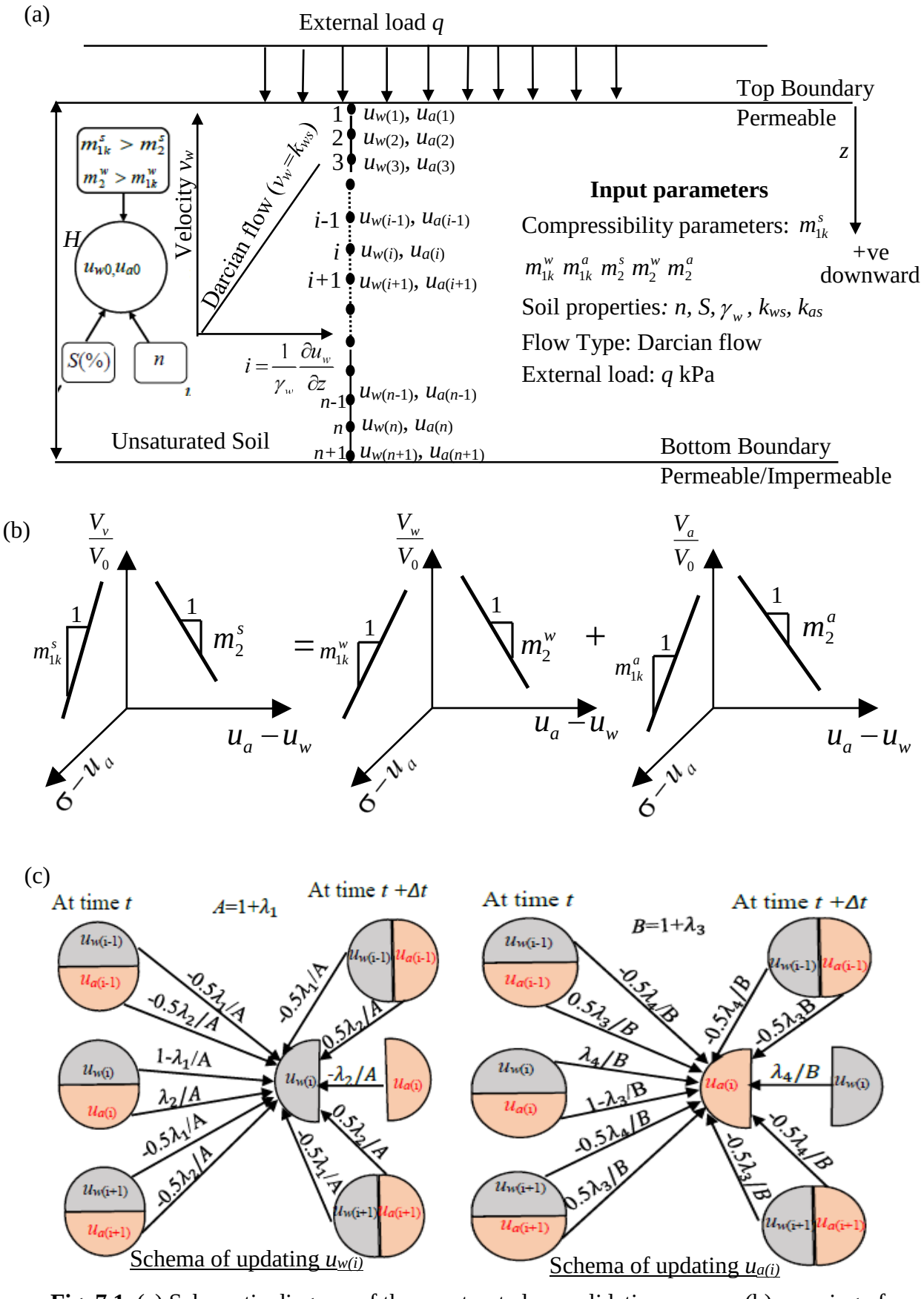

Fig. 7.1. (a) Schematic diagram of the unsaturated consolidation process (b) meaning of compressibility parameters (c) schema of updating $u_{w(i)}$ and $u_{a(i)}$.

The mathematical expressions of all the considered distributions are given in Chapter 3 and are not repeated here. This chapter focuses primarily on understanding the impact of the various generated PAP and PWP profiles on the overall consolidation of unsaturated soil. Apart from the deviation from the uniform pore pressure (initial), the other assumptions of the conventional unsaturated analysis are retained. For the sake of completeness, the considered assumptions are summarized next.

7.2.1 Assumptions Involved

1. Soil solid and water particles are incompressible.
2. Water and air phases are continuous and interdependent. Since contractile skin volume change is internal to the element and soil particles are incompressible, the continuity equation can be written as: $\Delta V_v / V_0 = \Delta V_w / V_0 \quad + \quad \Delta V_a / V_0$ (7.1)

   Consequently, at any stress point: $m_{1k}^s = m_{1k}^w + m_{1k}^a$ and $m_2^s = m_2^w + m_2^a$ (7.2)
3. The effect of air diffusing through water, water vapor movement, and any other influence of environmental factors (such as temperature change and moisture flux boundaries) are ignored.
4. The air phase follows the ideal gas law; this indicates that all the internal energy is in the form of kinetic energy.
5. The nonlinear distribution of *S* above the ground water table is completely ignored and a constant value of *S* is adopted in the entire unsaturated zone.
6. The permeabilities of the water (k_{ws}) and the air (k_{as}) phases are homogenous and stress-states ($\sigma - u_a$ and $u_a - u_w$ both) independent.
7. The flow of water and air within the vadose zone is assumed to be governed by Darcy's (1856) law and Fick's (1855) linear law, respectively.

A) Darcy's law (water phase): $v_w = k_w.i$; $\quad i = \frac{1}{\gamma_w}\frac{\partial u_w}{\partial z}$ (7.3a)

Here, (i) v_w and k_w are the velocity (discharge velocity) and coefficient of permeability of the water phase, (ii) i and γ_w represent the hydraulic gradient and unit weight of water, respectively.

B) Fick's law (air phase): $\quad J_a = -D_a \frac{\partial u_a}{\partial z}$ (7.3b)

Here, J_a represents the mass rate of air flowing across a unit area of the soil and D_a indicates the stress-state independent transmissivity coefficient of the air phase. The diffusion of air in the vadose zone is well described by Fick's law without any existence of sharp boundaries as they are observed in non-Fickian diffusion. Conventionally, the concentration gradient is used in other disciplines for representing the Fickian transport. However, in unsaturated soil mechanics, it is postulated that the diffusion of air is proportional to the space gradient of pore air pressure, i.e., air flows from a high air-pressure zone to a low air-pressure zone.

8. The compressibility parameters are constant. During the transient process, when the stress increment is small, the assumption of constancy of the compressibility parameters is justifiable. Nevertheless, the changes in the void ratio and water content with respect to the stress state variables are nonlinear, and therefore, truly speaking, the stiffness parameters controlling the volumetric deformations are precisely variables.
9. The soil is stable-structured, i.e., the deformation moduli related to the water phase and the soil structure are negative. This implies, that the increase in stress state variables reduces void ratio and water content.
10. The settlement occurs along the loading direction i.e., vertical direction.

11. The load is applied instantaneously.
12. Considering the rigidity of the soil structure, the small strain theory is used.

7.2.2 Numerical Formulations

Following Fredlund and Rohardjo (1993), the expressions of transient flow are obtained by equating the time derivative of the volume change constitutive equations (related to the water and air phase) to the divergence of the flow rate of the corresponding phases. The derivations of the one-dimensional uncoupled governing dissipation equations are detailed in Appendix E3. The flow laws and the constitutive relations are exclusively used to derive the governing equations of both phases.

Governing Differential Equations (GDEs):

$$\text{For water phase: } \frac{\partial u_w}{\partial t} = \frac{1}{1 - C_a C_w}\left(c_v^w \frac{\partial^2 u_w}{\partial z^2} - C_w c_v^a \frac{\partial^2 u_a}{\partial z^2} \right) \tag{7.4a}$$

$$\text{For air phase: } \frac{\partial u_a}{\partial t} = \frac{1}{1 - C_a C_w}\left(c_v^a \frac{\partial^2 u_a}{\partial z^2} - C_a c_v^w \frac{\partial^2 u_w}{\partial z^2} \right) \tag{7.4b}$$

Subjected to: (a) Initial conditions: $u_j(z,0) = u_{j0}(z)$ [Different for Cases A–J] (7.5)

(b) Boundary conditions: $u_j(0,t)=u_j(H,t)=0$ for PTPB (7.6a)

$u_j(0,t)= 0 \quad \frac{\partial u_j}{\partial z}(H,t) =0$ for PTIB. (7.6b)

j will be replaced by *w* and *a* for the water and air phases, respectively.

It is to be noted that in the conventional consolidation analysis of saturated homogenous soil, only one material parameter (c_v) is associated with the spatial derivative (2nd order) of excess PWP, whereas, in the unsaturated soil a total of four coefficients exists in the GDE. The parameters, C_w and C_a, are non-dimensional, whereas, the dimension of c_v^w and c_v^a is L^2T^{-1}.

7.2.3 Solution Strategy

The parabolic PDEs are solved through the Crank-Nicolson (CN) scheme of the finite difference method. Firstly, the soil stratum is discretized with (n+1) number of equally spaced grid-points. Unlike the saturated soils, each node exhibits (a) two unknowns (u_w and u_a), and (b) two governing equations. Hence, there will be (2n-2) numbers of unknowns for PTPB and 2n numbers of unknowns for PTIB. Appendix E4 presents the discretization of the two expressions, by using the semi-implicit scheme, for any arbitrary i^{th} node. Upon simplification, the discretized linear algebraic equations can be represented in compacted form as: $G \times U^{t+\Delta t} = H^t$. Four non-dimensional coefficient parameters - two (λ_1, λ_2) for the water phase and two (λ_3, λ_4) for air phase equations- form the building block of the coefficient (known) matrix, G, and right-hand side known vector, H. The unknown vector U comprises the unknown variables, u_w and u_a. It is noteworthy that the G matrix remains constant throughout the analysis. The update of the U-vector occurs due to the change in the elements of the H-vector at each time step.

7.3 RESULTS AND DISCUSSION

The results are represented in six different forms: (a) generation of maximum initial excess PWP (u_{w0}) and PAP (u_{a0}), (b) normalized isochrones (of excess PWP and PAP), (c) trace of the spatial position of maximum pore pressures (u_{jmax} path) with time, (d) consolidation curve (U_{javg} vs time), (e) variations of normalized pore pressures (u_j /u_{j0max}) at a few specific locations, and (e) temporal variation of rate of dissipation ratio (RDR_j). Throughout this chapter, the subscript "j" indicates the respective phases. Except for the first segment, the other results are presented for the following fixed set of parameters: (a)

Air (k_{as}) and Water (k_{ws}) Permeability: $k_{ws}= k_{as}=10^{-10}$ m/sec,

Coefficient of volume compressibility: $m_{1k}^{s} = -2.5\times10^{-4}$ kPa $^{-1}$, $m_{2}^{s} / m_{1k}^{s} = 0.4$,

$m_{1k}^{w} / m_{1k}^{s} = 0.2$, and $m_{1k}^{w} / m_{2}^{w} = 0.25$

Degree of saturation (S): S=0.80

Porosity (n): n=0.5

Applied Pressure: q=100 kPa

7.3.1 Development of u_{w0} and u_{a0}

Fig. 7.2 shows the variation of initially induced undrained excess pore fluid pressures generated for an uncoupled analysis with respect to various soil parameters. The magnitude of u_{w0} and u_{a0} decreases with the (a) increase in porosity, and/or (b) decrease in saturation level. Irrespective of the influencing factors, the value of u_{a0} is smaller than that of u_{w0}. The variation of the saturation (S) level in the lower range has a very minimal impact on the developed u_{w0} and u_{a0} values. For instance, corresponding to n=0.5, when S changes from 10% to 50%, u_{w0} and u_{a0} increase by 9.25% and 73%, respectively; whereas, surprisingly when S elevates from 50% to 100%, u_{w0} and u_{a0} shoots up by 219.26%, and 1096.56%, respectively. The compressibility parameters, especially those related with the water phase, are supposed to have noticeable influences on the induced excess pore pressures; m_{1k}^{w} is related to the water generation ability due to the mechanical stress and m_{2}^{w} indicates the specific water capacity due to the matric suction. Higher values of m_{2}^{w} result in remarkably lower magnitude of u_{w0}; nevertheless, the variation in u_{w0} appears to be less affected by the parameter m_{1k}^{w} .

7.3.2 Isochrones and u_{max} path

The curves are represented in terms of non-dimensional parameters. The vertical axis depicts the normalized depth (z/H), while the horizontal axis shows the magnitude of

u_j normalized with respect to the applied load u_{j0}; j represents the fluid phase. The depth at the bottom layer is denoted by 'H'. In this context, u_{j0max} refers to the maximum value of

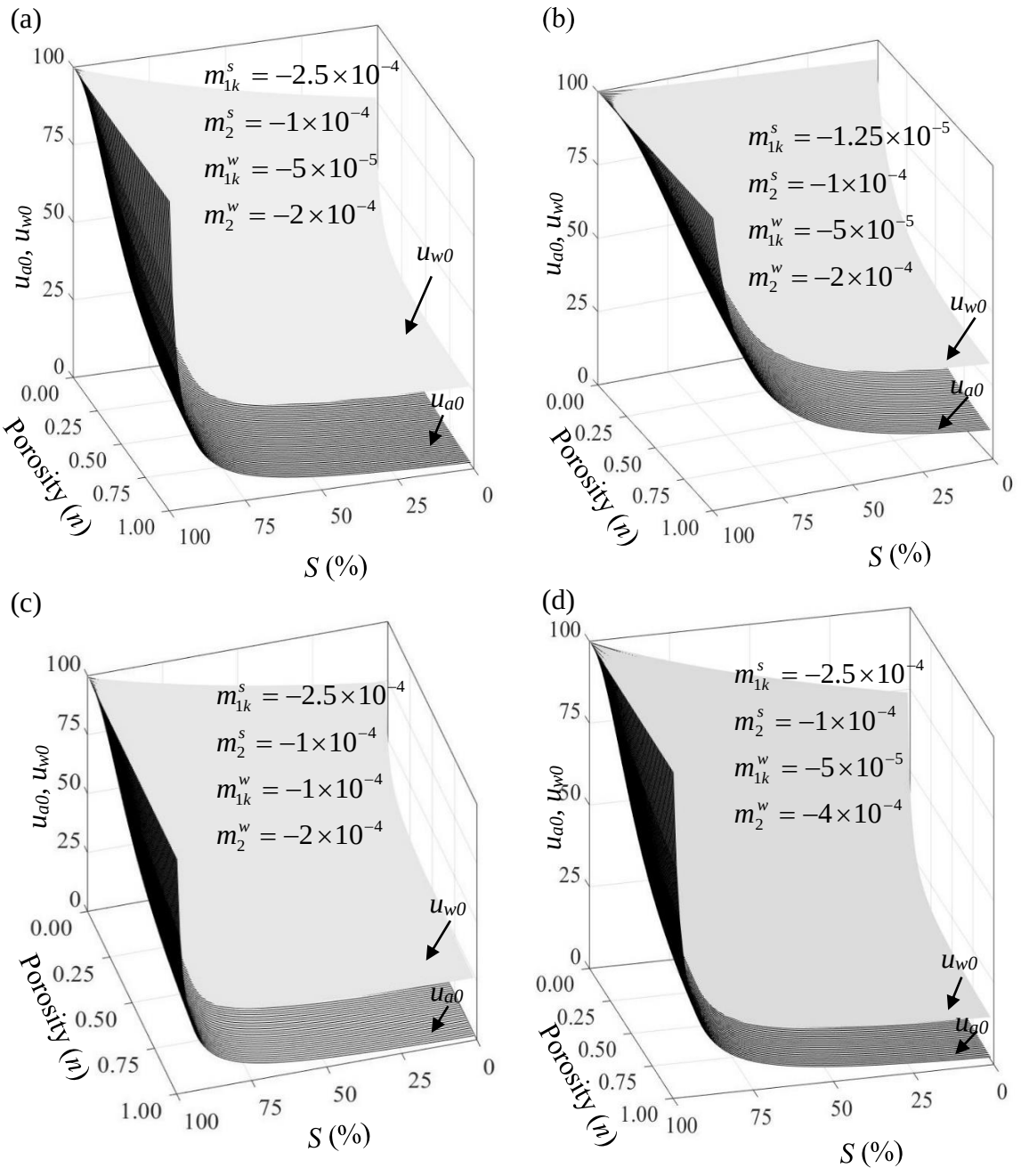

Fig. 7.2. Variation of the initial excess pore water and pore air pressures with respect to saturation, porosity, and corresponding to various compressibility parameters, namely, (a) initial, (b) $5\times m_{1k}^{si}$, (c) $2\times m_2^{si}$, (d) $2\times m_2^{wi}$; here, initial set indicates $m_{1k}^{si} = -2.5a, m_{1k}^{wi} = -0.5a, m_2^{si} = -a, m_2^{wi} = -2a$ with a=10^{-4} and the other compressibility parameters in b, c, and d are the same.

pore water pressure generated by the applied load q. Figs 7.3 and 7.4 illustrate the isochrones for various u_{j0} distributions at different time values (0.5, 2.5, and 5 months) for PTPB and PTIB boundary conditions, respectively.

The initial excess pore pressure distributions (u_{w0} and u_{a0}) are represented by solid lines, and other isochrones (except t =0) by dotted lines. Owing to the assumption of infinite velocities at the drainage boundaries, 100% consolidation is achieved at the pervious boundaries, resulting in zero pore pressures at those boundaries throughout the process. Despite both the air and water phases having the same permeability, the air phase dissipates much earlier than the water phase.

From Figs 7.3 and 7.4, it is observed that for symmetric initial pore water pressure distributions (Cases A, B, F, and H), the isochrones for both air and water phases remain symmetric, forming a sinusoidal shape for PTPB and a half-sinusoidal (increasing) shape for PTIB conditions throughout the process. In contrast, for asymmetric cases (Cases C, D, E, G, I, and J), the isochrones initially become skewed for a certain period before becoming sinusoidal and half-sinusoidal for PTPB and PTIB, respectively. In some cases (Fig7.3: Cases I and J; Fig 7.4: Cases B, D, E, F, H, I, and J), pore pressures (u_w and u_a) start to accumulate in certain portions rather than dissipation. This is evidenced by the isochrones that intersect and cross the u_{w0} curves over a certain period. The rise in the pore pressures mainly happens near the bottom drainage boundary and is predominant for PTIB cases. This behaviour can be attributed to the redistribution of the pore pressures, as discussed before for the saturated case.

Like Chapter 3, the u_{max} paths, representing the locus of the maximum pore pressures, are drawn on the isochrone graphs. Two u_{max} paths – one for the air phase and the other for the water phase– are illustrated here. The isochrones and the u_{max} paths for the air and water phases are represented in red and black color, respectively. Fig 7.3 presents

the u_{max} paths corresponding to PTPB conditions. For symmetric distributions (Cases A, B, F, and H) u_{max} paths, regardless of fluid phases, are horizontal and pass through the midpoint of the consolidating layer. On the contrary, the u_{max} paths for asymmetric distributions (Cases C, D, E, G, and J), start from the maximum point of the u_{j0} profiles and head toward the midsection, and eventually exhibit a horizontal plateau at the mid-portion. The horizontal u_{max} path through the central portion of the consolidating layer indicates the generation of the symmetric isochrones during the end stage of the consolidation. For Cases C, D, E, and G the turning of the u_{max} path is gradual towards the central portion. However, for arched and skewed distribution, a sudden change happens towards the central portion. A remarkable difference is observed between the u_{max} path generated from the air and the water phase only for the skewed distributions. For the other type of u_{j0} distributions, the u_{max} paths for air and water phases are coincident. The u_{max} paths for the PTIB condition tend towards the bottom undrained boundary. Fig7.4 shows that the u_{max} paths corresponding to Cases A, C, and G, where, u_{j0max} is at the bottom, are horizontal and pass through the bottom of the consolidation layer. The journey of the u_{max} path through the bottom undrained layer shows the development of the half-sinusoidal isochrones, which are observed in the conventional PTIB consolidation analysis.

7.3.3 U_{avg} versus time

The global picture of consolidation can be represented by the U_{avgj} versus time curve. In saturated condition U_{avg} is also indicator of degree of settlement because volume changes only because of the expulsion of water. But in case of unsaturated soil mechanics the total volume change of soil depends upon the volume change due to the expulsion of water and air phase (soil particles is assumed to be incompressible).

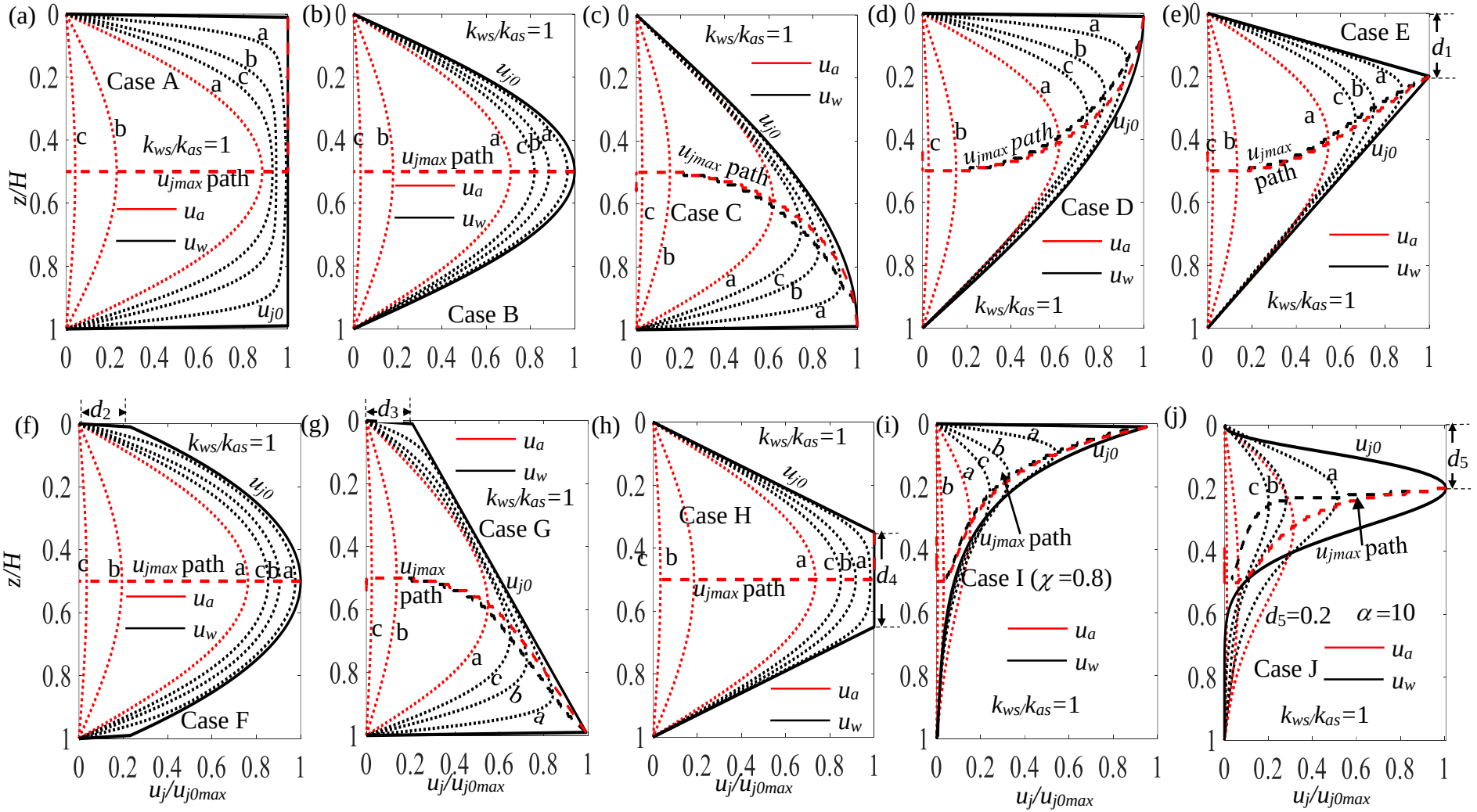

N.B.: (i) a, b, and c represents the consolidating isochrones @ T equals to, 0.5, 2.5, and 5 month, respectively

Fig. 7.3 Spatial distributions of u_j (isochrones) and u_{jmax} path for PTIB and corresponding to the following u_{j0} distributions:(a) uniform (b) sine (c) and (d) half sine increasing and decreasing (e) mid angle triangular (f) parabolic (g) and (h) trapezoidal (i) arched (j) skewed

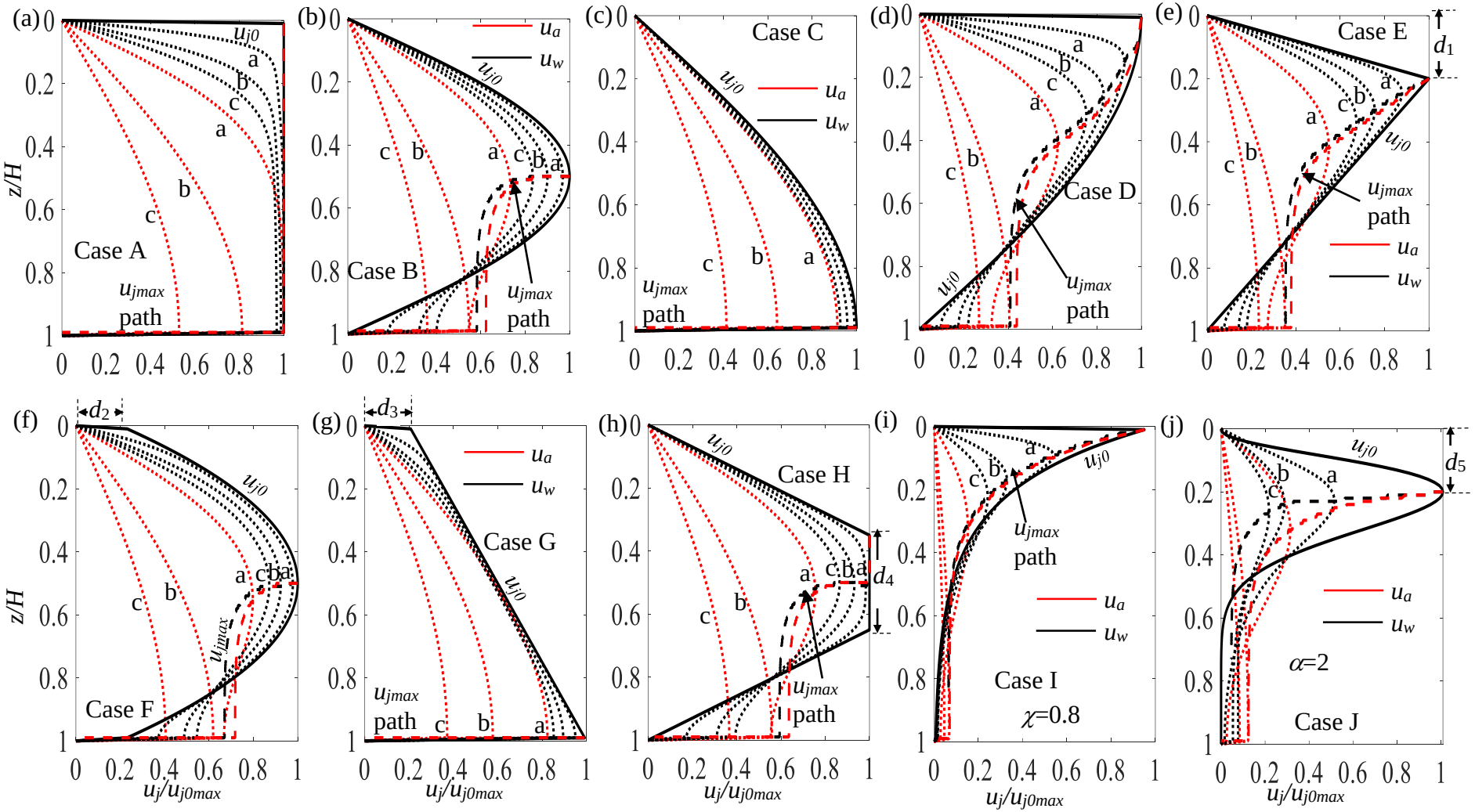

N.B.: (i) a, b, and c represents the consolidating isochrones @ T equals to, 0.5, 2.5, and 5 month respectively

Fig. 7.4 Spatial distributions of u_j (isochrones) and u_{jmax} path for PTIB and corresponding to the following u_{j0} distributions:(a) uniform (b) sine (c) and (d) half sine increasing and decreasing (e) mid angle triangular (f) parabolic (g) and (h) trapezoidal (i) arched (j) skewed

In unsaturated soil, U_{avg} for water phase and air phase are independent to each other and represented as:

$$\text{For water Phase } U_{avgw} = 1 - \frac{\int_0^H u_w(z,t)dz}{\int_0^H u_w(z,0)dz} \qquad \text{For air phase } U_{avga} = 1 - \frac{\int_0^H u_a(z,t)dz}{\int_0^H u_a(z,0)dz} \qquad (7.7)$$

Figs. 7.5 and 7.6 illustrate the variation of the average degree of consolidation (U_{avgj}) with time (t) for PTPB and PTIB conditions, respectively. From these figures, it is evident that the air phase dissipates much faster than the water phase. The effect of the shape of the initial excess pore water pressure is similar for both phases.

From Figs. 7.5a, and 7.6a, it can be observed that there is no effect of d_3 parameter (refer to Case G) on the rate of consolidation for PTPB case, while in PTIB boundary condition d_3 affects the temporal variation of U_{avgj} to a noticeable extent at the mid-stage of consolidation. As the value of d_3 increases, the rate of consolidation increases.

Figs. 7.5b and 7.6b represent the effect of the trigonometric distribution of u_{j0}. The nature of the half-sinusoidal u_{j0} distributions (Cases C and D) does not appear to have any role in the consolidation curve as long as the top and bottom boundaries remain drained. On the contrary, the sinusoidal u_{j0} distribution slows the consolidation rate in the initial stage and then expedites the dissipation process and coincides with the Cases C and D-induced consolidation curve. For the PTIB condition, the consolidation curve for Case B remains in between Cases C and D; the U_{avgj} vs t-curves Case manifests a faster rate of consolidation. For Case E, the variation of d_1 does not mark an appreciable impact on the consolidation curves generated from the PTPB condition; nevertheless, the change in d_1 manifests discernible differences in the consolidation curves for the undrained bottom boundary condition. Under PTIB conditions, the rate of consolidation seems higher if the apex of the triangular u_{j0} distribution is adjacent to the pervious (top) boundary.

Cases F and H show a similar pattern- increasing the values of d_2 and d_4 decreases the rate of consolidation for both PTPB and PTIB conditions. The curvature (χ) of the arched distribution (Case I) influences the overall consolidation tremendously. Irrespective of the drainage boundaries, a slight change of the χ -parameter massively impacts the consolidation rate - the higher the χ, slower the consolidation rate.

Figs. 7.5f and 7.6f demonstrate the influence of the d_5 (the normalized depth of the skewed distribution from the top surface) and α (the degree of skewness) parameters on the consolidation curves. It is observed that compared to α, d_5 plays a crucial role in dictating the form of U_{avgj} vs t-curves for both drainage boundary conditions. The rate of consolidation increases if most of the initial excess pore water pressure is concentrated near the drainage surface. By viewing Figs. 7.5 and 7.6, it can be broadly concluded that the shape of the u_{j0} distribution is more influential when the concerned clays are subjected to a one-way drainage boundary.

7.3.4 Variation of pore pressure with time at different height

Figs. 7.7 and 7.8 represent the variations of normalized pore pressures over time at specific locations – (a) 20% below the top surface (z/H=0.2), (b) mid-section (z/H=0.5), and (c) 20% above the bottom surface (z/H= 0.8); the normalization is done with respect to $u_{j0,max}$. These figures provide a local perspective of the pore pressure distributions. The pore pressure profiles are plotted for both phases (air and water) and both drainage boundaries (PTPB and PTIB). Except for Cases I and J, the u_a and u_w profiles corresponding to other u_{j0} distributions, in PTPB, exhibit a flat horizontal plateau upto a considerable amount of time and then tend towards the zero pore pressure line. For Cases I and J with PTPB condition there are noticeable undulations on the horizontal sections of u_a and u_w profiles.

However, for PTIB condition, the wavy nature of the horizontal sections of u_a and u_w profiles are viewed for various cases: Cases B, D, E, I, and J.

The undulations of the horizontal sections indicate the redistribution of pore pressures which happens mainly for the arched and skewed distribution, especially for the PTIB condition. For symmetric u_{j0} distribution, the u_a and u_w profiles corresponding to z/H=0.2 and z/H=0.8 coincide with each other. The dissipation of air pressure at any location happens much ahead of the dissipation of water pressure.

7.3.5 Rate of dissipation with time

The change in the dissipation rate between any assumed non-uniform u_{j0} distribution with the conventional rectangular u_{j0} distribution is compared through the *rate of dissipation ratio* (RDR_j) (Lovisa and Sivakugan (2014)). RDR_j is defined as follows:

$$RDR_j = R_{1j}/R_{0j} \tag{7.8}$$

where, R_1 and R_0 denote the normalized area of undissipated excess PWP attained at any arbitrary time during consolidation for non-uniform and uniform u_{j0} distribution, respectively, and is expressed as follows:

$$R_1 = \frac{\left[\int_0^H u_j(z,t)\right]_{non-uniform}}{\left[\int_0^H u_j(z,0)\right]_{non-uniform}} \quad ; \quad R_0 = \frac{\left[\int_0^H u_j(z,t)\right]_{uniform}}{\left[\int_0^H u_j(z,0)\right]_{uniform}} \tag{7.9}$$

Figs. 7.9 and 7.10 illustrate the trend of the RDR_j over time for PTPB and PTIB conditions, respectively. These graphs provide insight into how quickly or slowly the consolidation process progresses over time when the initial excess pore water pressure (PWP) is non-uniformly distributed, compared to the conventional assumption of a uniform distribution.

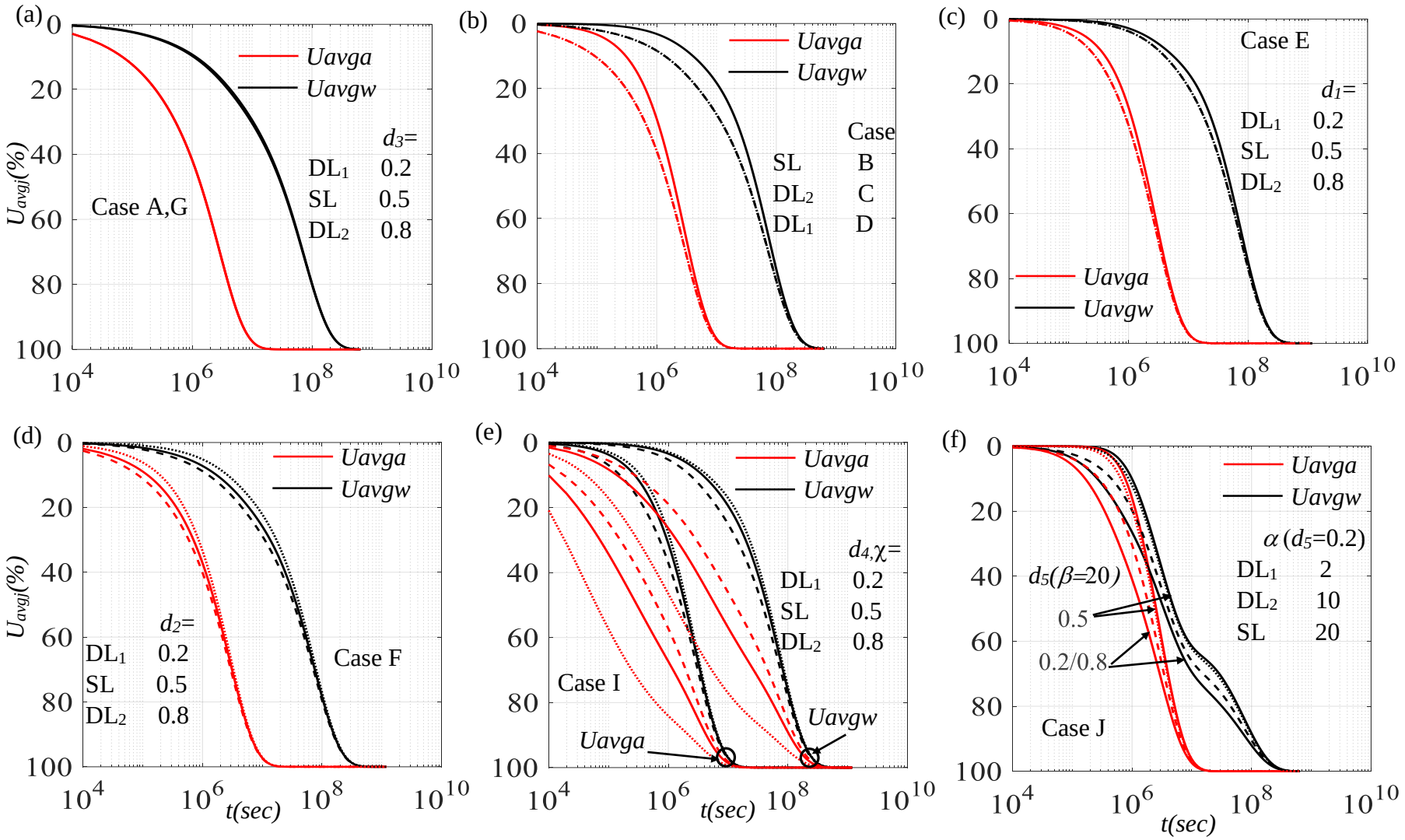

N.B.: (i) DL_1, DL_2, and SL represents the Dotted, Dashed and Solid line, respectively.

Fig. 7.5 Consolidation curve corresponding for various u_{j0} distributions subjected to two way drainage.

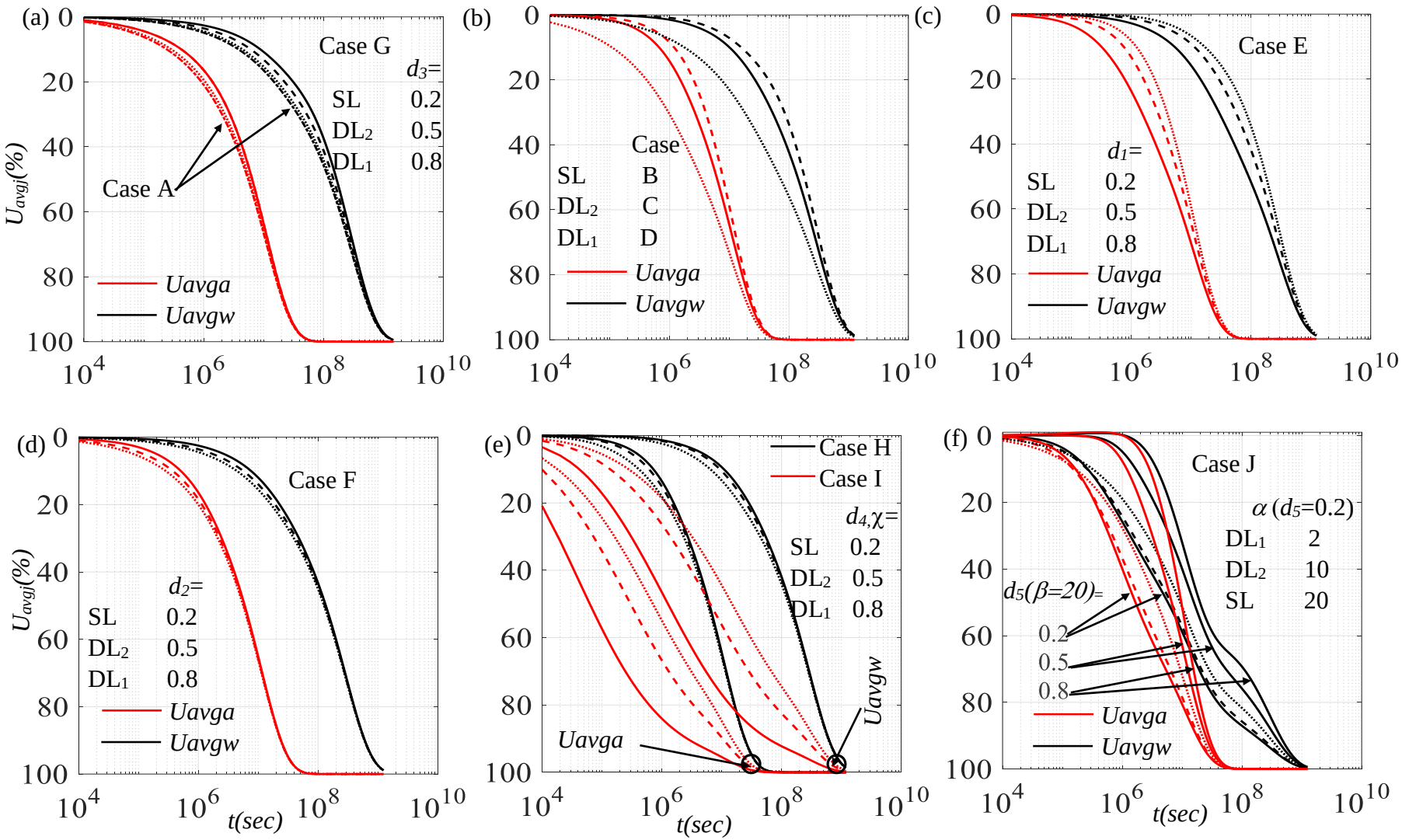

N.B.: (i) DL_1, DL_2, and SL represents the Dotted, Dashed and Solid line, respectively.

Fig. 7.6 Consolidation curve corresponding for various u_{j0} distributions subjected to one-way drainage.

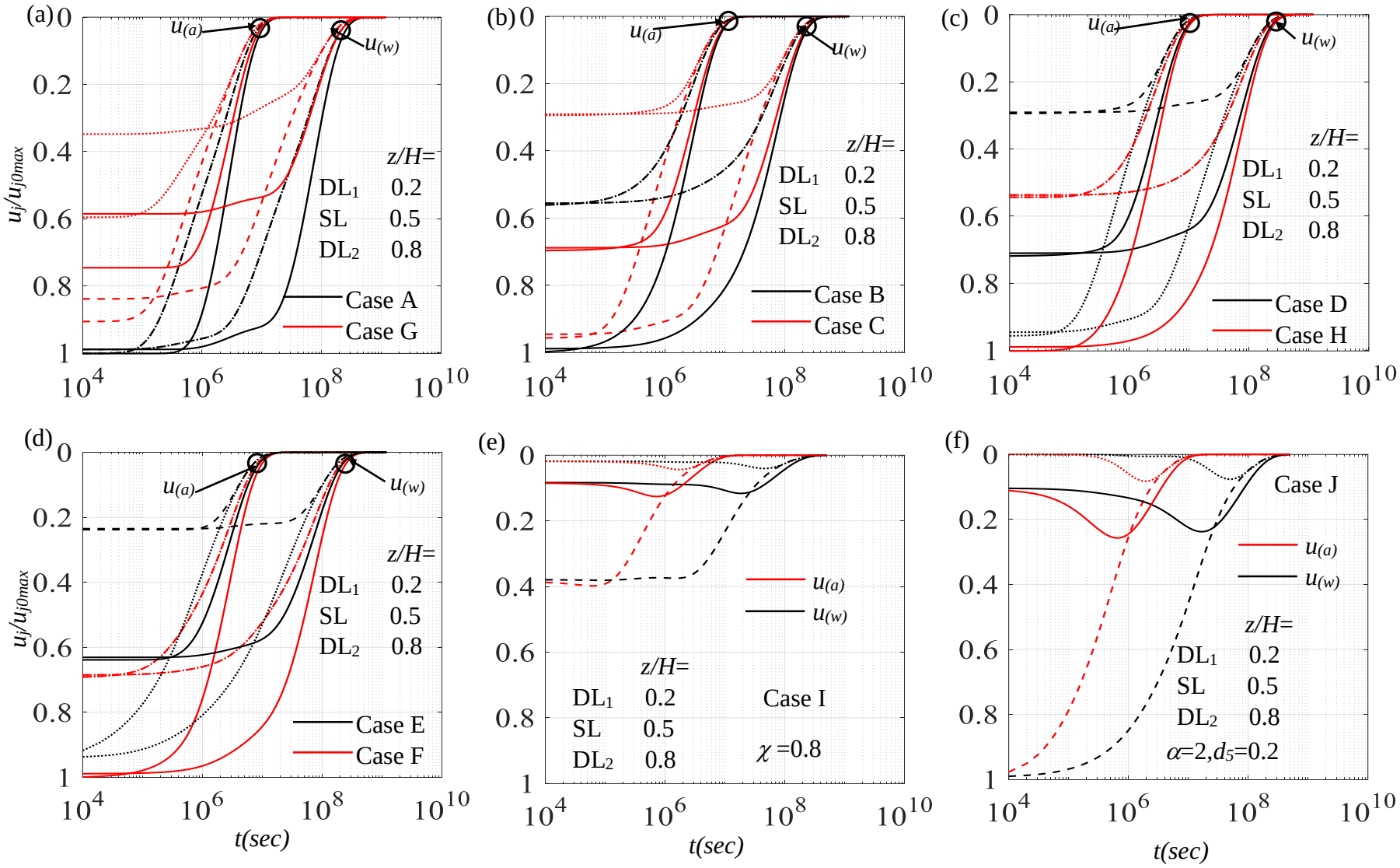

N.B.: (i) DL_1, DL_2, and SL represents the Dotted, Dashed and Solid line, respectively.

Fig. 7.7 Variation of normalized pore pressure with time at different depth (2m, 5m and 8m) subjected to PTPB boundary condition.

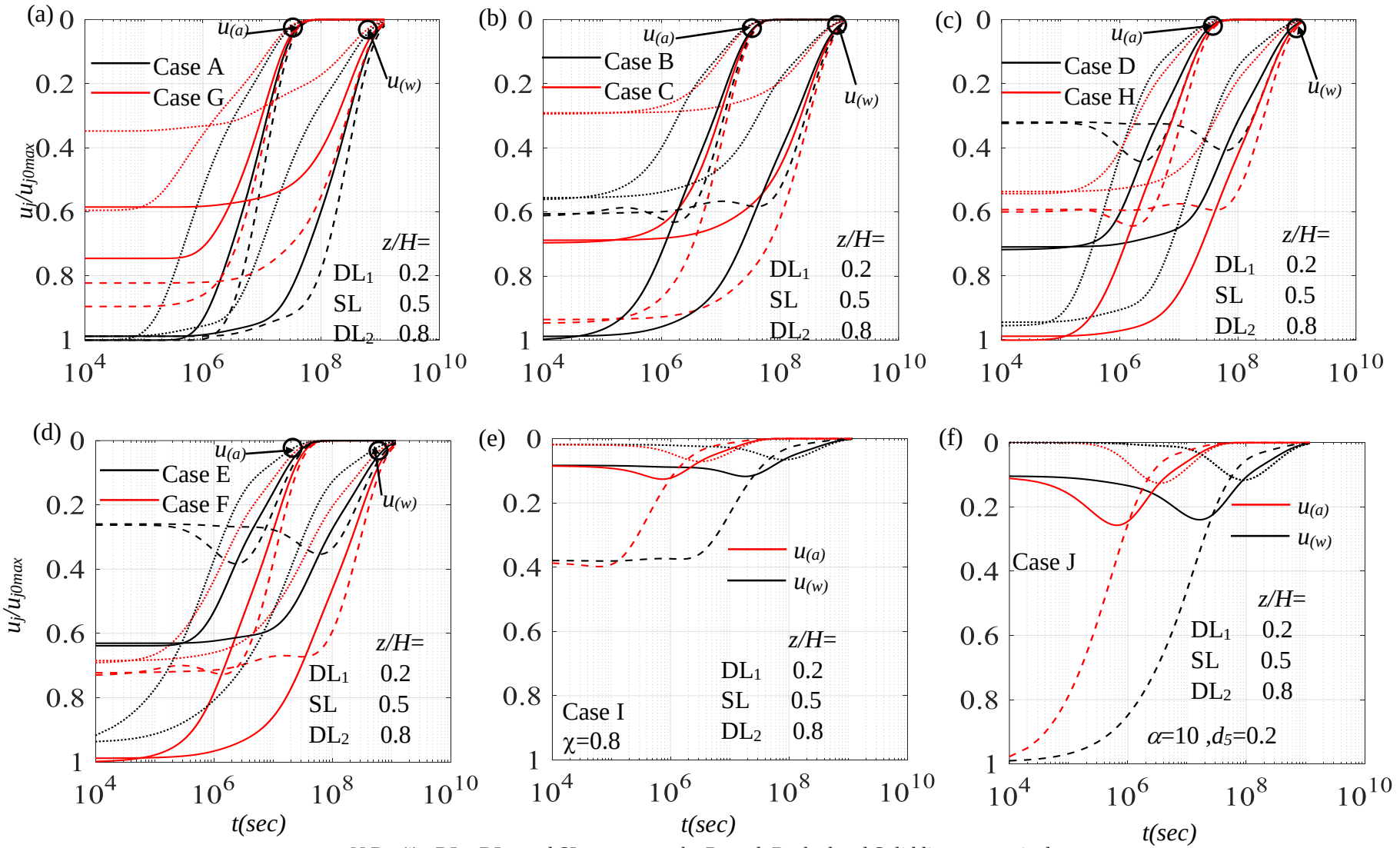

N.B.: (i) DL_1, DL_2, and SL represents the Dotted, Dashed and Solid line, respectively.

Fig. 7.8 Variation of normalized pore pressure with time at different depth (2m, 5m and 8m) subjected to PTIB boundary condition..

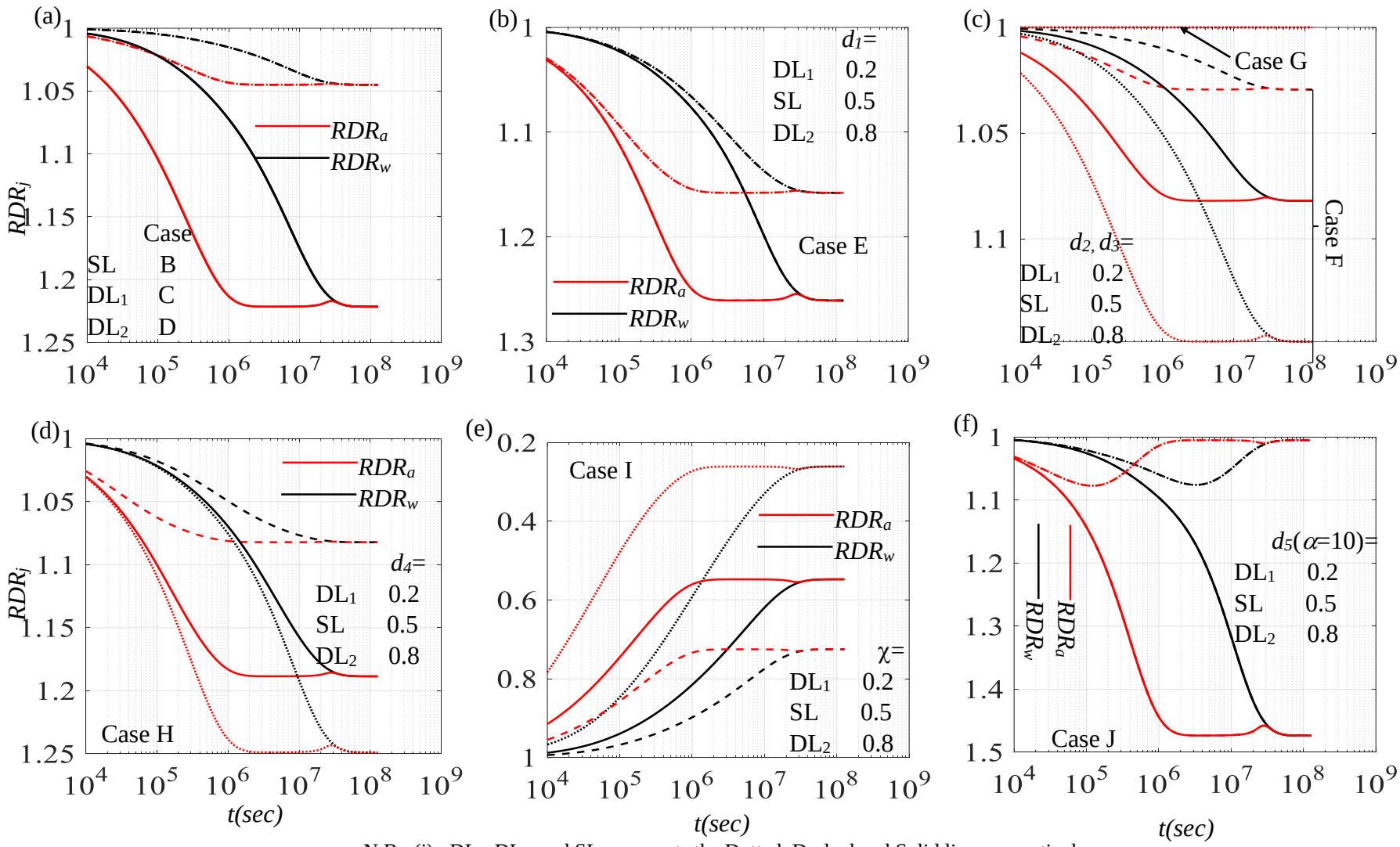

N.B.: (i) DL_1, DL_2, and SL represents the Dotted, Dashed and Solid line, respectively.

Fig. 7.9 RDR_j curve for corresponding to various u_{j0} distribution curve for PTPB boundary condition.

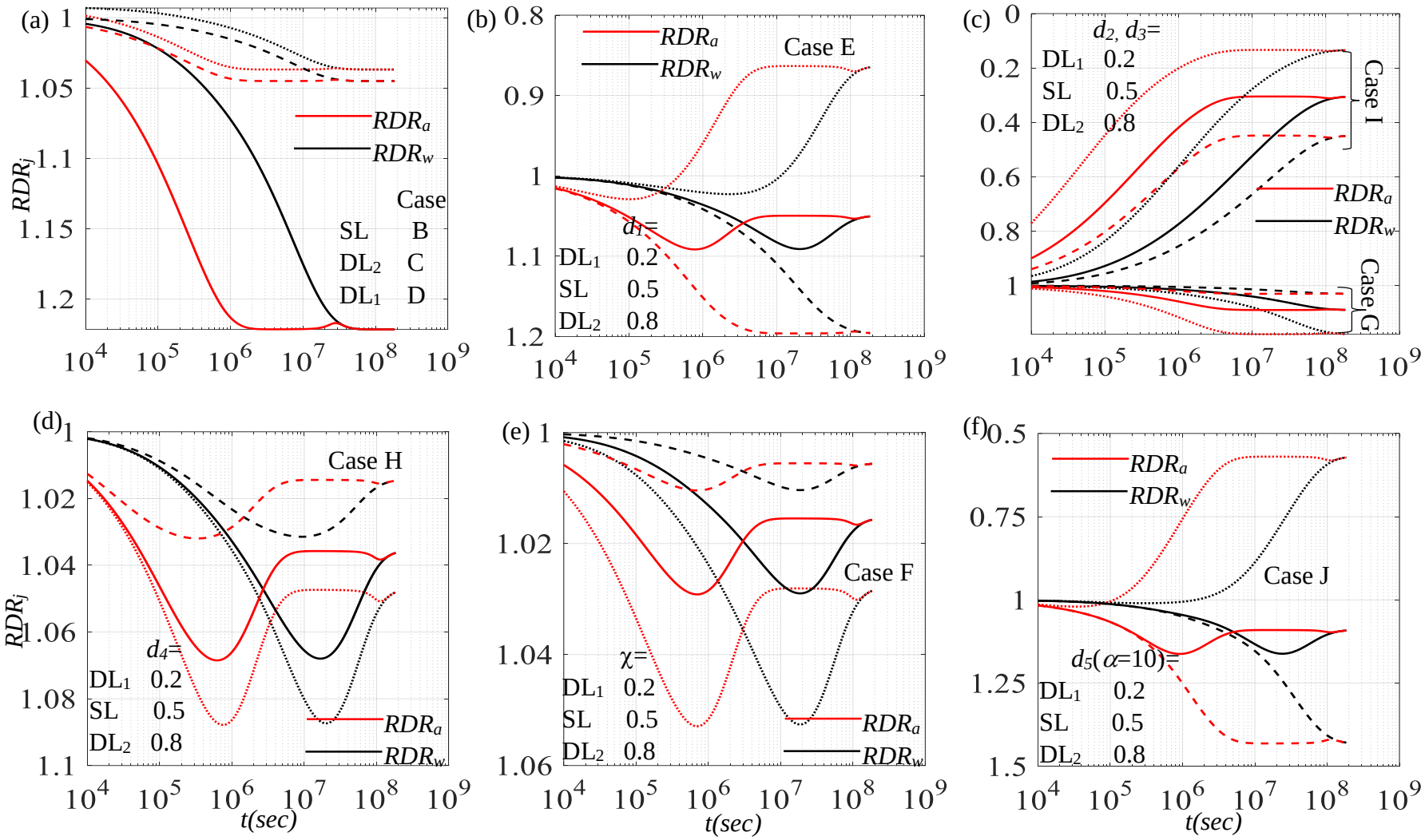

N.B.: (i) DL_1, DL_2, and SL represents the Dotted, Dashed and Solid line, respectively.

Fig. 7.10 RDR_j curve for corresponding to various u_{j0} distribution curve for PTIB boundary condition.

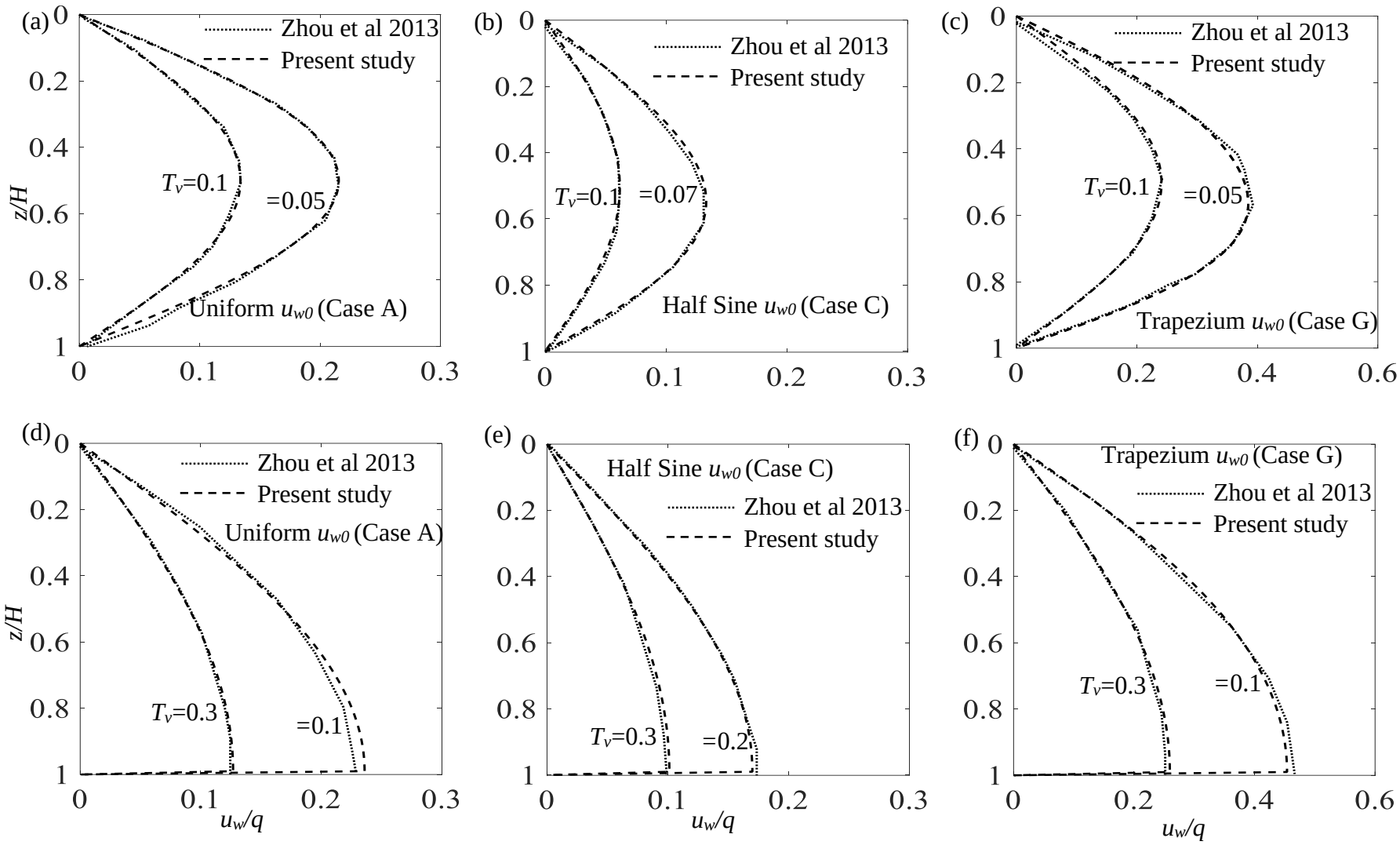

Fig. 7.11 The verifications of the present solutions on the basis of normalized isochrones with Zhou et al (2013).

The figures reveal that RDR_j is highly dependent on the shape of the initial PWP and the drainage condition. If RDR_j is less than 1, the rate of consolidation is faster than for a uniform initial PWP distribution; if RDR_j is greater than 1, the rate is slower. Fig 7.9 indicates that for any value of the length parameters (e.g., d_1, d_2, d_3, and d_4), Cases B, C, D, E, F, and H have RDR_j values consistently higher than 1. This means that the rate of dissipation is lower in these cases compared to a uniform u_{j0}. In Case G, RDR_j equals 1 for all values of d_3, which is why the U_{avg} curve for a uniform u_{j0} merges with this case. Case I shows RDR_j values lower than 1 for all parameters, indicating that the rate of dissipation is always higher than for a uniform u_{j0} . Case J has RDR_j values greater than 1 for all values of d_5. Fig 7.10 presents interesting trends in RDR_j, for Cases B, C, D, F, G, and H, RDR_j is always greater than 1, while for Case E and Case J, it depends on the shape of u_{j0}. For Case I, RDR_j is always less than 1.

7.4 VALIDATION

Fig 7.11 shows the comparison of the present numerical solutions with the analytical solutions reported by Zhou et al (2013) for PTPB and PTIB drainage conditions for a uniform, trapezium, and half-sine distribution. The range of deviations between the present computed solutions and the solutions of Zhou et al (2013) is a maximum 0.01% - 5%). The close proximity between these solutions provides the necessary confidence in the methodology and the written code.

7.5 SUMMARY

This chapter demonstrates the impact of various symmetric as well as asymmetric initial pore pressure (water and air) distributions on the overall consolidation of an unsaturated clay (homogenous) layer. Following Fredlund and Rohardjo (1993), there are two partial differential (governing) equations – one for the water phase and the other for

the air phase – that control the consolidation behaviour of the vadose zone. An uncoupled analysis is performed with the help of Crank-Nicolson semi-implicit method. The only difference from the conventional unsaturated consolidation analysis by Fredlund and Rohardjo (1993) is the incorporation of different initial conditions. The analyses are carried out for two PTPB as well as PTIB drainage boundary conditions. The findings are depicted in terms of normalized isochrones, consolidation curves, temporal variations of PAP and PWP for certain specific points, and rate of dissipation ratio. The phenomenon of pore pressure redistribution occurs significantly for one-way drainage boundaries with non-linear asymmetric initial distributions.